scientific reports

Check for updates

OPEN

A 903-year annual temperature reconstruction for the southeastern tibetan plateau from the tree ring widths of *Juniperus saltuaria*

Shanshan Xu[1], Chaogang Zheng[1], Zhiyuan Shang[1,2,3]✉, Zhigang Zhang[1,2,3], Xinggong Kong[1,2,3], Iain Robertson[4] & Zhijun Zhao[1,2,3]✉

Precisely dated paleoclimatic records are essential for understanding natural and anthropogenic climate influences. Here, an annually resolved absolutely dated *Juniperus saltuaria* tree ring width chronology from the Haizi mountain, southeastern Tibetan Plateau (TP) was developed. The chronology shows the annual- to decadal-scale paleoclimatic variability of the southeastern TP over the past 903 years (1115–2017 CE). The tree ring widths correlate significantly with mean annual temperature (T_{mean}). A linear regression model between ring width and T_{mean}, accounting for 57% of the variance in temperature from 1959 to 2017 CE, was used to reconstruct the past 903 years of T_{mean} variation in the southeastern TP. The chronology aligns with other temperature records from the TP, Asia, and the Northern Hemisphere (NH), indicating a marked temperature increase since the late twentieth century, with 1998–2017 CE identified as the warmest period. The coldest thirty years occurred in 1115–1145 CE. Solar activity and the Atlantic Multidecadal Oscillation exert notable influences on temperature fluctuations in this region. Superposed epoch analysis indicates that volcanic eruptions had significantly impacted southeastern TP temperatures, causing dramatic cooling for 2–4 years. Our study presents the longest width chronology developed by *Juniperus saltuaria* to date, offering a long-term perspective on recent climatic shifts across the southeastern TP. This work enhances understanding of historical climate variability, providing critical insights to refine projections of future climate variability.

Keywords Tree rings, Tibetan Plateau, Paleoclimatology, Mean temperature, Last millennium

Knowledge of multidecadal global mean surface temperature (GMST) fluctuations, as well as their relative magnitudes compared with that of the projected long-term warming trend, is essential for anticipating future climate change dynamics[1]. Exactly dated climate archives for the last millennium are required to evaluate the increasing impact of human activity. Simultaneously, better understanding the workings of the climate system as a whole can enhance our capacity to predict future climate changes[2,3]. Numerous studies in recent decades suggest that warming amplification in high-elevation regions is an intrinsic feature of recent global warming, and find a significant altitudinal amplification trend for the Tibetan Plateau (TP)[4]. As one of the most unique geographical features in the world, the TP has been recognized as one of the tipping points of the climate system, which can affect the climate change in East Asia and the rest of the world[5]. Therefore, it is key to understand the history and dynamics of climate on the TP since global warming is causing immediate and disastrous effects on the ecosystem of the TP[6]. However, instrumental records from meteorological stations on the TP are sparse, only a limited temporal perspective on natural climate variability is provided, and few stations have meteorological records prior to the 1950s which is too short to investigate long-term climate oscillations on the TP[7]. Therefore, dated climatic proxies, such as stalagmites, lake sediments, ice cores, pollen and tree rings, have been widely used for climate reconstructions[8,9,10,11,12]. Among them, tree-rings are widely regarded as one of the most reliable proxies of past environmental information[13]. This is due to their ability to offer

[1]School of Geography, Nanjing Normal University, Nanjing 210023, China. [2]Jiangsu Centre for Collaborative Innovation in Geographical Information Resource Development and Application, Nanjing 210023, China. [3]Key Laboratory of Virtual Geographic Environment, Ministry of Education of China, Nanjing 210023, China. [4]Department of Geography, Swansea University, Singleton Park, Swansea SA2 8PP, UK. ✉email: shangzy@njnu.edu.cn; zhaozhijun@njnu.edu.cn

annually resolved, reliable, and precisely dated climate data, making them valuable for analyzing long-term climate fluctuations[14]. The southeastern TP belongs to subtropical alpine canyon region where characterized with complicated terrain, including low-latitude plateaus and longitudinal valleys[15]. The climate of this region is under the influence of the westerly and monsoon circulations of the Indian and Pacific Oceans[16]. As a result, accurately characterizing the weather and climate in this region is both important and challenging. Fortunately, the southeastern TP offers an ideal location for dendroclimatological research due to its extensive coverage of alpine coniferous forests[17]. These forests exhibit high sensitivity to climate change, making them valuable for studying and understanding climatic variations[18]. Numerous dendrochronological studies have investigated TP regional temperature variability[19,20,21,22,23,24,25,26]. These records, however, are mostly concentrated on the last 200 to 400 years, and there is only one long chronology (longer than 900 years) that reflects temperature changes. Bräuning et al. combined of 24 individual tree-ring chronologies to established a 1400-year-long tree-ring chronology to investigate historical temperature variability on the southeastern TP, but they failed to carry out appropriate calibration and verification testing between tree-ring width and climate data[27]. Later, Wang et al. developed a mean annual temperature reconstruction covering the period 984–2009 CE in Qamdo City, Tibet Autonomous Region, China[23]. Multi-century and millennial records with high resolution and good dating control in the southeastern TP, however, remain scarce. Hence, long-term variability in annual temperature in this region needs to be given more attention.

The conifer, *Juniperus saltuaria* Rehder & E. H. Wilson, has great potential for paleoclimate reconstruction. In its upright growth form, *Juniperus saltuaria*, reaches a height of around 9 m, and the canopy density is 30%-50%[17]. As a unique subtropical evergreen coniferous tree species native to the eastern and southern TP, *Juniperus saltuaria*has a long growth period, considerable age, clear tree rings, few false rings and missing rings, making it highly suitable for establishing millennial chronologies[26]. However, there have been few relevant studies using *Juniperus saltuaria*as a proxy to reconstruct climate[28,29]. Additionally, these studies have resulted in relatively short chronologies, such as the 172-year T_{mean}chronology for the Wolong Natural Reserve in Sichuan province, China, developed by Li[30] and the 170-year T_{min}chronology in our study area developed by Zou[26].

In this study, we report an annually resolved, absolutely-dated *Juniperus saltuaria* tree ring width chronology for Haizi mountain in the southeastern TP (Fig. 1). The objective of this study was to (1) develop the longest

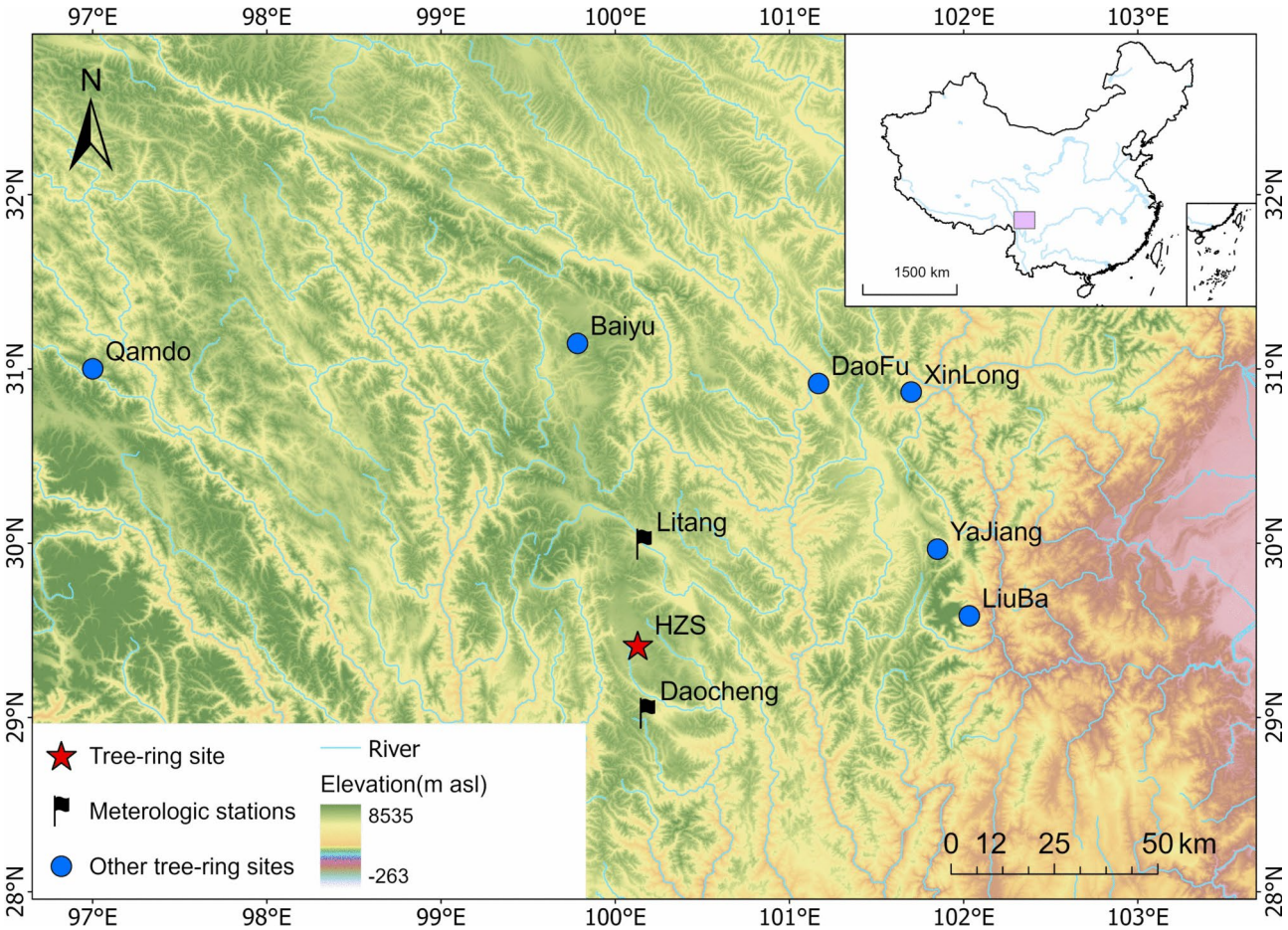

Fig. 1. Location of our sampling sites (red pentagram) and the other sampling sites used in this study on the southeastern TP (blue dots). The black flags in the map show the location of the meteorological stations. The figure is plotted using the ArcMap (Version 10.7).

tree-ring width chronology based on *Juniperus saltuaria*, (2) provide further information on long term climate variability in the southeastern TP, and (3) examine the influence of external forcing factors such as volcanic eruption, Atlantic Multidecadal Oscillation (AMO) and solar activity, and (4) explore the effect of large explosive eruption (Volcanic Explosivity Index, VEI > 5) on the temperature of the southeastern TP.

Results

Climatic-growth response

A tree-ring chronology for *Juniperus saltuaria*of 903 years in length, from 1115 to 2017 CE, was constructed. Sections of the chronology with fewer than eleven cores were truncated to eliminate weak replication. The mean segment length, or the average number of rings per core, was 630 years. The relatively low interannual variability of the chronology was expressed by the mean sensitivity value (0.19) and low standard deviation (0.14). The value of first-order autocorrelation coefficient (AC1) for the chronology was relatively high (0.71), suggesting that annual growth is affected by the growth of the previous year (biological persistence)[14]. The relatively high level of signal-to-noise ratio (SNR, 7.23) indicated that the trees constituting the mean chronology had strong common signals. In addition, the standard chronology (STD) shows an obvious low-frequency variation on decadal and multidecadal scales.

The relationships between ring-width index and climate data which include P, T_{mean}, T_{min}, and T_{max} were explored from the previous January to the current December over the common period 1959–2017 (Fig. 2a). The chronology correlated positively with T_{mean} and T_{min}, whereas it was weakly correlated with precipitation and T_{max}. It should be noted that the correlation with T_{min} of each month all reached 99% confidence level. The result indicated that, at this site, it was temperature that limited tree growth rather than precipitation.

Based on the single-month analysis, T_{mean} and T_{min} were selected for the multi-monthly correlation analysis (Fig. 2b, 2c). The results showed that all correlation coefficients between chronology and T_{mean} exceeded the 99% confidence level in different time periods. The positive correlations were largest in previous August to current July (0.76, $P < 0.01$), and strong positive correlations were also shown for the T_{mean} from the previous October to the current September (0.75, $P < 0.01$). Furthermore, the strong influence of mean temperature during the previous October to the current September had certain physiological meaning. The results of this study demonstrated that T_{mean} is the primary limiting factor affecting the growth of local *Juniperus saltuaria*.

Mean annual temperature reconstruction

Based on the relationships between ring-width index and climate data, the mean temperature for the period from the previous October to the current September was chosen for reconstruction. By using the regression analysis method, we established the linear regression equation between the STD chronology and temperature as follows.

$$T_{poct\text{-}csep} = 2.25 \times STD + 2.45.$$

Where $T_{poct\text{-}csep}$ represents the reconstructed value of the mean temperature from previous October to current September, and STD means the *Juniperus saltuaria* tree ring index in our study area. As shown in Table 3, the predictor variable accounted for 59% of the variance of annual temperature of the predict and still accounted for 57% after adjusted. Both of the regression coefficients passed the significance test, which indicated that the model fit well and the equation had high reliability. The 'leave-one-out' crossing-test method was used to test the validity of our linear regression model, reduction of error (RE) and coefficient of efficiency (CE) values were positive, the product means test (t) was 7.38, which indicated that the reconstruction equation had passed the test. The correlation between the reconstructed temperature and the measured temperature from 1959 to 2017 CE was 0.75 ($P < 0.01$). The observed and reconstructed annual temperature in the southeastern Tibetan Plateau during the period 1959–2017 CE are shown in Fig. 3a. The overall trend of the reconstructed temperature had good coherence with the measured temperature. All these factors demonstrated that our reconstruction equation was stable and it could generally represent the mean annual temperature of this region.

Analysis of change characteristics of reconstruction sequence

Using the linear regression equation constructed above, a mean annual temperature reconstruction from 1115 to 2017 CE is presented (Fig. 3b). Cubic spline smoothing with 11-year wave length was used to reveal low frequency variations at the decadal scale. The reconstructed mean annual temperature during 1115–2017 CE was 4.64 ℃ and the root mean square error was 0.50. The T_{mean} series for the past 903 years shows low-frequency fluctuation. In this region, T_{mean} tended to increase since 1115 CE, and reached the peak of 5.64 ℃ in 1157 CE. After a warm period of almost half a century, the temperature fell abruptly and a cold period occurred in the 1200 s. The end of the thirteenth century to the middle of the sixteenth century was a relatively warm period which was followed by a rapid decrease over the middle of the sixteenth century. The temperature was relatively stable during 1620–1749 CE, then decreased rapidly at the end of the eighteenth century and the beginning of the nineteenth century. Since 1850s, the reconstructed mean temperature exhibited an upward trend. The mean annual temperature was high in the first half of the twentieth century and early 21th century, but 1960–1997 CE was a cold period. The warmest and coldest years were 2010 CE and 1818 CE respectively, with respective temperatures of 5.88 °C and 3.52 °C. The warmest period in the past 903 years was 1998–2017 CE, with the mean temperature being 0.45℃ higher than that in 1115–2017 CE. The coldest decade occurred in 1115–1145 CE, during which the mean temperature was only 4.25 ℃, 0.39 ℃ lower than it in 1115–2017 CE. Based on 11-year low-pass filter, the period above and below the mean temperature for 11 consecutive years was regarded as the warm episode and cold episode respectively. The reconstructed T_{mean} showed that nine warm episodes and nine cold episodes occurred during the past 903 years (Table 4).

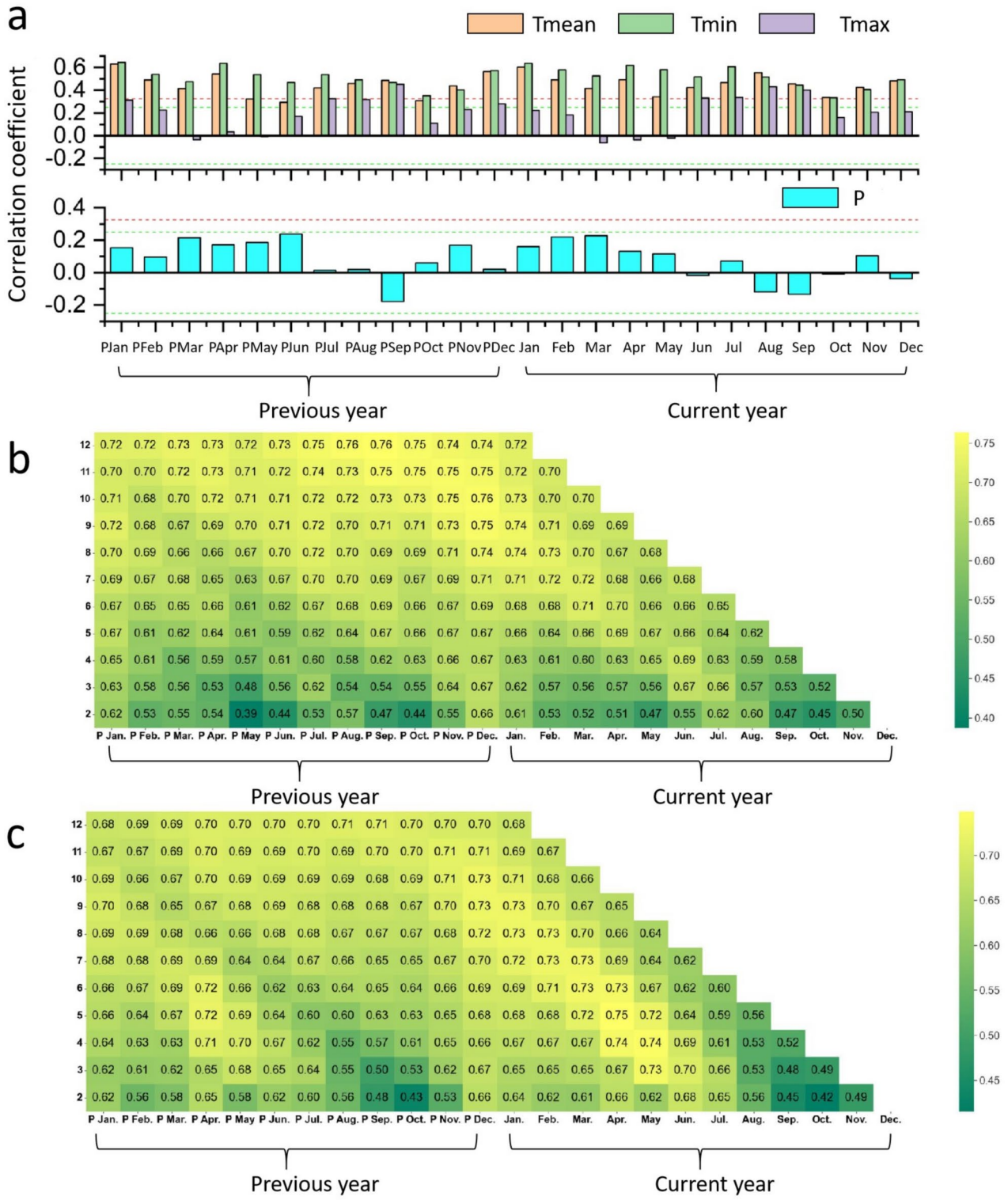

Fig. 2. Correlation analysis between ring-width index and climate factors from 1959 to 2017. (a) shows the correlation between the tree-ring width index and monthly precipitation (P), mean temperature (T_{mean}), mean minimum temperature (T_{min}), and mean maximum temperature (T_{max}) from previous January to current December, the green dashed line denotes the significance at 95% level; the red dashed line denotes the significance at 99% level. The correlation coefficients between the tree-ring width index and multi-month variations of mean temperature are shown in (b), and mean minimum temperature in (c), with the y-axis representing multi-month combinations (e.g., "2" refers to the mean data from previous January to February, "12" refers to the mean data from previous January to December).

Number	Date	Type	# C/T	Mean series length	Time span	Elevation (m a.s.l)	Latitude	Longitude
HZS1	2020/7/26	disc	20	630a	787–2017 CE	4500–4550	29.41°N	100.13°E
HZS2	2019/7/18	core	73/30	365a	1114–2019 CE	4500–4600	29.41°N	100.13°E

Table 1. Basic information of the sampling sites. # C/T = number of core and tree.

Chronology statistics				Common interval analysis					
Time span	MS	SD	AC1	Common period	SNR	PC1	EPS	CWT	CBT
1115–2017 CE	0.19	0.14	0.71	1640–1990 CE	7.23	18.6%	0.88	0.16	0.43

Table 2. Standard tree-ring chronology statistics. Note: MS (mean sensitivity), SD (standard deviation), AC1 (the first-order auto-correlation), SNR (signal–noise ratio), PC1 (the first principal component %), EPS (expressed population signal), CWT (Mean correlation within trees), CBT (Mean correlation between trees).

Time span	R^2	Ra^2	ST	RE	CE	t
1959–2017	59%	57%	47 + 14 −	0.46	0.46	7.88

Table 3. The validation of the reconstructed temperature. Leave-one-out validation statistics for the common period 1959–2017. R^2 (the variance), Ra^2 (the variance after adjustment), ST (sign test), RE (reduction of error), CE (coefficient of efficiency), t (the product means test).

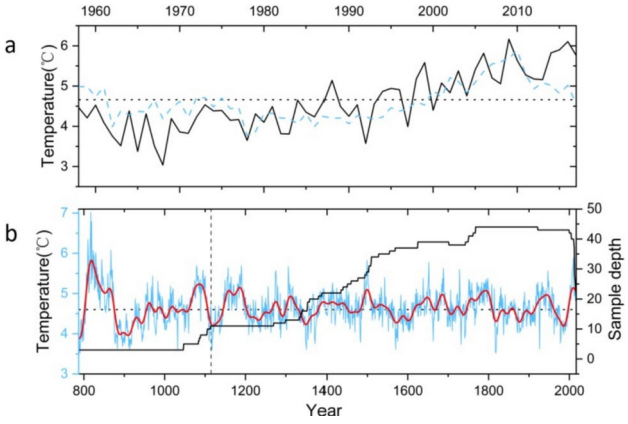

Fig. 3. (a) Comparison between observed (solid line) and reconstructed (dotted line) annual temperature in southeastern Tibetan Plateau during the period 1958–2017 CE. Horizontal dotted line indicates the mean value of the meteorological record. (b) Reconstructed mean annual temperature departures relative to the whole series for the southeastern Tibetan Plateau with the degree of replication. The smoothed (red) line is the 11-year fast Fourier transform (FFT) filter.

Warm period		Cold period	
Span(years)	Anomaly value (℃)	Span(years)	Anomaly value (℃)
1146–1201(56)	0.37	1115–1145(31)	− 0.39
1267–1282(16)	0.20	1202–1266(65)	− 0.20
1301–1327(27)	0.19	1283–1300(18)	− 0.18
1382–1448(67)	0.12	1328–1381(54)	− 0.24
1485–1547(63)	0.17	1449–1484(36)	− 0.12
1618–1698(81)	0.15	1548–1617(70)	− 0.24
1747–1808(62)	0.29	1699–1746(48)	− 0.11
1916–1959(44)	0.26	1809–1915(107)	− 0.17
1998–2017(20)	0.45	1960–1997(38)	− 0.31

Table 4. The warm/cold period in 1115–2017 CE on Haizi mountain.

Discussion

Annual temperature signals encoded in *Juniperus saltuaria* tree-ring widths

The positive correlation of tree rings with temperature and the lack of a significant correlation with precipitation (Fig. 2a), indicates that *Juniperus saltuaria*is temperature limited. This climatic response pattern can be explained by stand condition and biotic factors. Firstly, the main limiting factor to tree growth will be influenced by altitude since precipitation gradually increase with increasing altitude while temperatures decrease. Our samples were collected at the tree line area at an altitude of about 4500 m a.s.l. At this altitude, precipitation is no longer a limiting factor for tree growth. Secondly, from the point of view of tree physiology, temperature influences the division and enlargement of cell and influences xylem lignification during the summer[31]. At the same time, lower summer soil temperatures can limit the growth of roots and their function in water uptake, thereby limiting tree growth in our study area. The warmer climate in spring also has a significantly positive effect on tree growth, higher spring temperatures can extend the growth season by breaking dormancy and boosting the division of tree cambium cells in advance[36,37], and increasing leaf area to increase the photosynthetic rate[34]. A warmer winter may protect the needles from frost damage and prevent root damage caused by freezing embolism, and maintain them photosynthetically active for the next year. However, in a cold winter, deep frost in the soil can delay thawing, thereby shortening the growing season. With less time to form new wood, trees produce narrower rings[35,36]. This climatic response model has been widely reported for many areas of the southeastern TP[15,37,38]. In conclusion, annual temperature signals encoded in *Juniperus saltuaria* growing on the Tibetan surface, and this climatic response pattern can be explained by stand condition and biotic factors.

Validation of the reconstruction

Spatial correlations confirm that our reconstruction can represent regional temperature variations[39]. The correlation between tree rings and Climate Research Unit (CRU TS4.08, 0.5° × 0.5°) data set for the period 1959–2017 CE (Fig. 4a, 4b) and 1901–2017 CE (Fig. 4c, 4d) shows that the reconstruction can be taken as representative of southeastern TP or even the entire TP. Spatial correlation fields are consistent for the instrumental (Fig. 4a) and reconstructed temperatures (Fig. 4b). The correlation after removing linear trends from the data are still significant for the entire TP.

The reliability of our mean annual temperature reconstruction is further confirmed by comparing with previous temperature series of the southeastern TP, including a winter T_{min} sequence in the past 345 years reconstructed by *Picea balfouriana*in western Sichuan Plateau[40], an early summer (June-July) T_{max} sequence in the past 563 years reconstructed by *Abies squamata Mast.*in Shaluli mountain[41], and an annual T_{mean} sequence reconstructed by *Sabina tibetica Kom.*in Qamdo in the past 1026 years[23]. All series have been smoothed by cubic spline smoothing with 11-year fast Fourier transform (FFT) filter (Fig. 4e, 4f). Common warm (cold) periods were found in these reconstructions, and the variations of these reconstructions were consistent: common warm periods occurred in the 1630–1650 CE, 1719–1731 CE, 1916–1959 CE, and cold periods occurred in the 1699–1718 CE, 1895–1915 CE, 1960–1980 CE. Common warm (and cold) periods were also found in other reconstructions[42,43]in the southeastern TP. However, there were deviations in some periods, for instance, in the seventeenth century, differences were found in our chronology and the chronology reconstructed by Wang et al.(2014a,b)[23]. For example, around 1600 CE, the two series change in opposite direction. These discrepancies may be caused by the heterogeneous microclimate environments among the study areas (our study site is located in Daocheng and the other is in Qamdo, 300 km away from ours), or because the detrending methods are different (A 67% of the series length cubic spline function used in our study and signal-free regional curve standardization used in Wang et al[23]. In addition, factors such as different period (monthly/seasonal/annual) of reconstruction and different species all can lead to inconsistent results. However, despite these minor differences, the overall trend is consistent.

Further comparisons were conducted between our reconstruction and other temperature reconstructions of the eastern TP[44], East Asia[45], and NH[46] over their common periods. The sequence reconstructed in this study agrees well with others (Fig. 4g), the correlation coefficients with NH, Asia and the eastern TP are 0.35 ($P < 0.01$), 0.22 ($P < 0.05$) and 0.23 ($P < 0.05$) respectively. Each sequence indicates that the temperature began to rise sharply in the second half of the twelfth century and then decrease sharply in the early thirteenth century. Temperature changes in the above regions were well consistent from the 11th to the fifteenth centuries, but from the mid-15th to the nineteenth centuries coherence became relatively insignificant and some discrepancies emerged. For example, in the early sixteenth century, the warm period in our reconstruction occurred about 20 years earlier than in other regions, in the late eighteenth century, the reconstructed temperature in this study was slightly higher than in other regions; in the mid-nineteenth century, the temperature in the TP was higher than in East Asia and NH. Although it was reported that the temperature of NH decreased in the second half of the twentieth century, the degree of cooling in the TP found in this study was more intense than the other sites in NH (Fig. 4g).

These discrepancies may be caused by the amplification of TP which can result in faster changes in intensity, duration and frequency of climate extremes[47]. In conclusion, our chronology is mostly consistent with other chronologies in the region. Various series have confirmed that the period from the 1960s to the 1990s experienced colder temperatures, followed by a significant temperature rise towards the end of the twentieth century. Although there may be slight variations in the magnitude and length of these changes, the overall trend remains consistent. The previous analysis suggests that the ring-width record of Haizi Mountain can serve as a reliable proxy of temperature fluctuations in the southeastern TP. It further indicates that during the past 903 years, temperature variations in the southeastern TP have generally followed the patterns observed in the NH.

The credibility of our chronology has been validated by historical records that contain valuable information. Documents displayed a cold phase in the period of the Southern Song Dynasty, roughly around the early twelfth

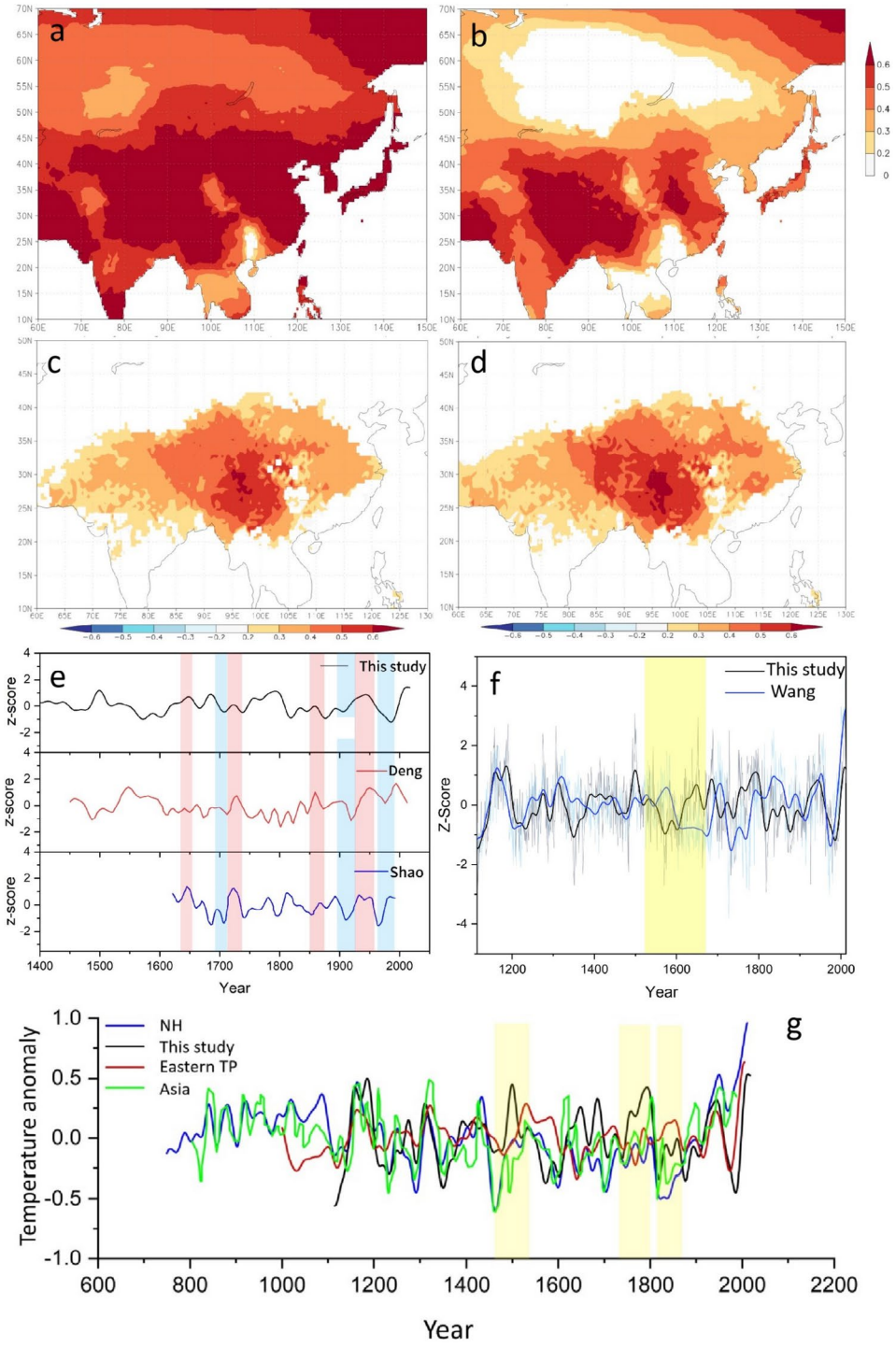

Fig. 4. Evaluation of temperature reconstruction reliability based on spatial correlations and comparisons with other climate records. Spatial field correlations between both instrumental (**a**) and reconstructed (**b**) mean annual temperatures (from previous October to current September) and regionally gridded temperatures for the period 1959–2017, as well as (**c**) correlations for the period 1901–2017, and (**d**) the spatial correlation patterns after de-trending for the extended 1901–2017. The figures (a-d) are created at http://climexp.knmi.nl. (**e**) Comparison of our annual temperature from the southeastern TP with winter T_{min} in the past 345 years (Shao)[37] and highest temperature change in early summer (June-July) during the past 563 years (Deng)[38]. (**f**) Comparison of our annual temperature reconstruction with the annual average temperature sequence of Qamdo during the past 1026 years (Wang)[20]. (**g**) Comparison of our temperature record (this study, black line) with temperatures from eastern TP (red line)[41], East Asia (green line)[42], and northern hemisphere (NH, blue line)[43]. The yellow shadows indicate the stage of divergence, and each sequence were obtained by cubic spline smoothing with a 11-year FFT filter.

century[48], this event align with the coldest period spanning from 1115 to 1145 CE. In addition, historical records indicate that from July to August in the year 1480, Yuexi in Sichuan province experienced both rain and snow, with the weather as cold as winter. Our reconstruction findings align closely with this event. These indicate that the cold period occurred not only in southeastern Tibet Plateau but also throughout China. Cai et al. conducted statistical analysis on the occurrence of freezing disasters in Shaanxi province during the Little Ice Age (LIA)[49]. This study showed the change of freezing disaster frequency was matched with the cold periods identified in our chronological reconstruction. These indicate that the cold period occurred not only in southeastern Tibet Plateau but also throughout China.

The coldest and warmest period during the past 903-year

Numerous studies have confirmed that the period from 1960 to 1990s was a cold period and this has been reported in previous studies (Fig. 4e). Moreover, the series reconstructed by Bräuning et al. indicated a decline of temperature during1970s–1990s[42]. Cook et al. showed that the summer temperature in the central Himalayas declined after 1960s[50]. The temperature reconstructions of many regions in the southeastern TP, such as Daxue Mountain, Shaluli Mountain, Wolong Mountain revealed that the 1960s–1990s was a cold period[53,]. This cold period might have been caused by the influence of Atlantic Multidecadal Variability (AMV) and volcanic eruptions. Shi et al. discovered that the TP is one of the few regions in Eurasia where minimum summer temperature can reflect AMV phase alternations during 1927–1994 CE[54]. In this period, there were three significant volcanic eruptions (1963, 1982 and 1991CE), which caused significant cooling across most regions of China[55]. Cold periods were also found in 1548–1617 CE and 1699–1746 CE during the LIA in our study area. The same results were also found in the vicinity of our sampling region such as Qamdo[23], Yajiang[56]and Litang[57]. Common cold periods during the LIA occurred in the first half of seventeenth and eighteenth century.

However, when it came to the coldest period of the past 903 years on a decadal scale, there were discrepancies between temperature reconstructions. In our research, the coldest three decades occurred in 1115–1145 CE instead of during the LIA (Fig. 3). Nevertheless, it is not entirely unprecedented, as similar results were also found in TP, the temperature anomaly among the TP showed that the temperature in the early twelfth century is lower than it in LIA[58]. In addition, the stable oxygen isotope ($\delta^{18}O$) records in Tibetan and in Guliya ice cores also support our conclusion[59]. But in many other studies the coldest period occurred in LIA, the results of these study showed that though the dramatic cooling experienced in the early twelfth century, average temperature during this period were still higher than during the LIA[23,]. Since the millennial records with high resolution and good dating control in the southeastern TP remain scarce, and the sample depth in this study in the early chronology is low, it is difficult to make a definite conclusion about this period.

According to the sequence reconstructed in our study, the mean temperature in the twentieth century was not the highest in the past 903 years. Although the temperature since the 1980s has risen rapidly, it has remained within the range of natural variability for the southeastern TP. The reason of this phenomenon may be due to the existence of a cold period from1960s to 1990s, which lowered the average of temperatures throughout the twentieth century. The mean temperature in the eighteenth century (4.75 ℃) was higher than that in the twentieth century (4.61 ℃). The mean annual temperature variability in the past 387 years of Renzhen town reconstructed by Yang et al. also showed that the warming in the twentieth century did not exceed the range of natural variability in the past 400 years[20]. However, on multidecadal or decadal scale, there was no doubt that the temperature had risen sharply since the end of the twentieth century, and many sequences showed a quickly warming trend[5253].

Possible linkage of temperature with external forcing

The result of multi-taper method (MTM) of spectral analysis reveal that the dominant periodicities are concentrated on 147, 36, 18, 7 and 2–2.6 years in our reconstruction (Fig. 5), of which the cycle of 147 and 2–2.6 years are the most significant. To investigate the roles played by large-scale internal modes of variability and different forcings on temperature in the southeastern TP over the past millennium, the correlations between our reconstruction and macroscale atmospheric circulations, including Atlantic Multidecadal Oscillation (AMO)[61], as well as radiative forcing from solar activity and volcanic aerosol were investigated[62,63].

The National Curriculum Development Center version 5 (NCDC V5) SST data were used to perform a correlation analysis with the annual T_{mean} during 1860–2017 CE (data from http://climexp.knmi.nl). The result showed that there is a significant positive correlation between T_{mean} in the southeastern TP and the SST of the North Atlantic, the North Pacific Ocean, Arctic and the Indian Ocean (Fig. 6a, 6b). The correlation between our reconstruction and NAO, PDO over the past 903-year is weak and insignificant (Fig. 6c), but it showed a significant correlation with AMO (Fig. 6d). This result supports the conclusion that the SST of the northern Atlantic could affect the decadal/multidecadal temperature variations of the TP through atmospheric bridges[25]. The correlation between positive/negative temperature anomalies and warm/cold AMO phases was illustrated (Fig. 6d). According to previous studies[23], the AMO affects temperatures on the Tibetan Plateau through two possible mechanisms. First, during warm phases, the AMO strengthens midlatitude westerlies, leading to negative surface air pressure anomalies over the North Atlantic and mid-latitude Eurasia[64]. This weakens the Siberian-Mongolian high-pressure system and reduces the strength of the East Asian winter monsoon, resulting in higher temperatures across East Asia[65]. Second, the AMO warms the middle and upper troposphere via a propagating Rossby wave train from the Atlantic to Asia[66]. Though the mechanisms linking the AMO to the Asian climate remain not fully clear, our finding implies that AMO variation is the important factor influencing temperature variability over the southeastern TP. But the relationship between AMO and temperature is not stable during the past 903 years. The correlation between AMO and temperature is insignificant during 1115–1300 CE, but it is significant during the 1300–2006 CE ($r = 0.27$, $P < 0.01$), especially during recent 200 years ($r = 0.41$, $p < 0.01$).

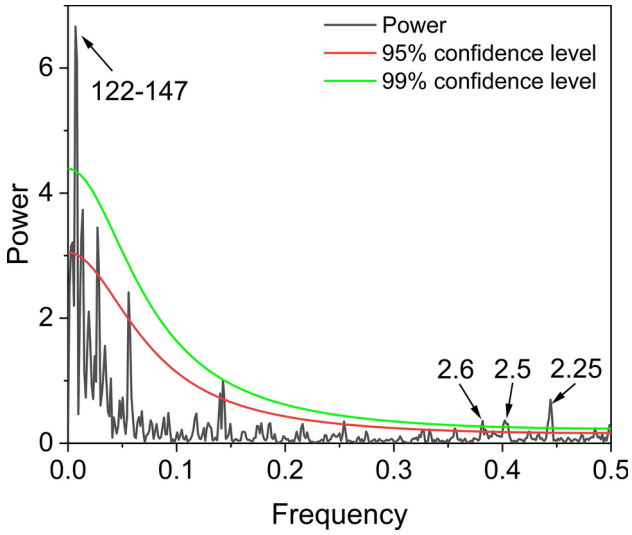

Fig. 5. The result of multi-taper spectrum of our reconstructed annual temperature, with 95% and 99% confidence level (CI confidence intervals) inferred from red noise spectra, and significant periods at 99% level are marked.

The role of volcanic eruption on the Earth's climate system and its influence has been widely discussed[67]. Previous studies have demonstrated that volcanic eruption played an important role in temperature change since the volcanic veil from explosive eruptions could influence climate change through atmospheric propagation of radiation[43]. Tree rings can reflect the impact of volcanic eruptions. Here, we explore the effect of large explosive eruption (Volcanic Explosivity Index, VEI > 5) on the temperature of the southeastern TP during the past 903 years. Volcano names, eruption dates, and eruption numbers are taken from the Volcanoes of the World database provided online by the Global Volcanism Program. According to the criteria (VEI > 5), the 16 strongest volcanic events are selected, 12 of which were in the NH and 4 in the Southern Hemisphere (SH) (Table 5).

The impact of volcanic eruptions on temperature variations in this study area is significant. For most years, large volcanic eruptions coincide with a drop in T_{mean} across the study area. Of the 16 strong volcanic eruption years, there are 14 event years in which temperature decreases in the event year or the following 1–3 years (Table 5, Fig. 7a). The results of SEA further support our conclusion, indicating a statistically significant cooling effect in the second year following the eruption, with temperatures remaining below average for an additional 2–4 years (Fig. 7b). Extremely powerful eruptions (VEI > 7) can cause a notable temperature drop[69], such as the volcanic eruption that occurred in 1257, where the temperature dropped by almost 0.9 °C, with the effect lasting approximately four years. The same result was also found in other research[70], such as Wang et al. found that out of 46 strong volcanic eruptions, 35 were followed by temperature decreases within this time frame[68]. Atmospheric aerosols resulting from volcanic eruptions affect temperature variations. Pinker et al. attributed the possible causes of global dimming to increasing anthropogenic aerosols and the lowering of atmospheric transparency following explosive volcanic eruptions[71]. Strong volcanic eruptions could send volcanic ash into the stratosphere with volcanic aerosols spreading throughout the world within a few months. The aerosols scatter some solar radiation and reflect some back to space, and then, the aerosols reduced the solar radiation reaching the ground[72]. The observed growth response may result from reduced tree photosynthesis because volcanic aerosols in the stratosphere intercepted incoming solar radiation.

When the periods of prolonged solar minima, such as the Spörer Minimum (1430–1520 CE) and the Dalton minimum (1780–1830 CE)[73], the cooling effect of the solar activity becomes dominant and leads to a drop in temperature. During the period around 1800 CE, solar activity was at the Dalton minimum, the AMO was in a cold phase, and there were frequent and intense volcanic eruptions were frequent. The combined effects of these three external forces resulted in a rapid decline in temperatures, ultimately leading to the relatively low temperatures observed between 1800 and 1900 CE. In conclusion, AMO, solar activities and volcanic eruptions have an important influence on the temperature change of TP.

Conclusions

An annually resolved, absolutely dated tree-ring width chronology for *Juniperus saltuaria* from Haizi Mountain in the southeastern TP is presented here, representing the longest chronology to date based on *Juniperus saltuaria*. Climate and tree growth relationship analyses show that the temperature significantly influences tree growth. A linear regression model between ring width and T_{mean}, accounting for 57% of temperature variance (1959–2017 CE), was used to reconstruct T_{mean} variation over the past 903 years in the southeastern TP. Spatial field correlations indicate that our reconstruction can represent large-scale mean annual temperature variability across the TP. The sequence shows similar warm-cold patterns to other reconstructions of the TP, Asia, and NH. The warmest period occurred in 1998–2017 CE, and the coldest period occurred in 1115–1145 CE. The sequence demonstrates multi-decadal, decadal and inter-decadal variations, with dominant periodicities are 147,

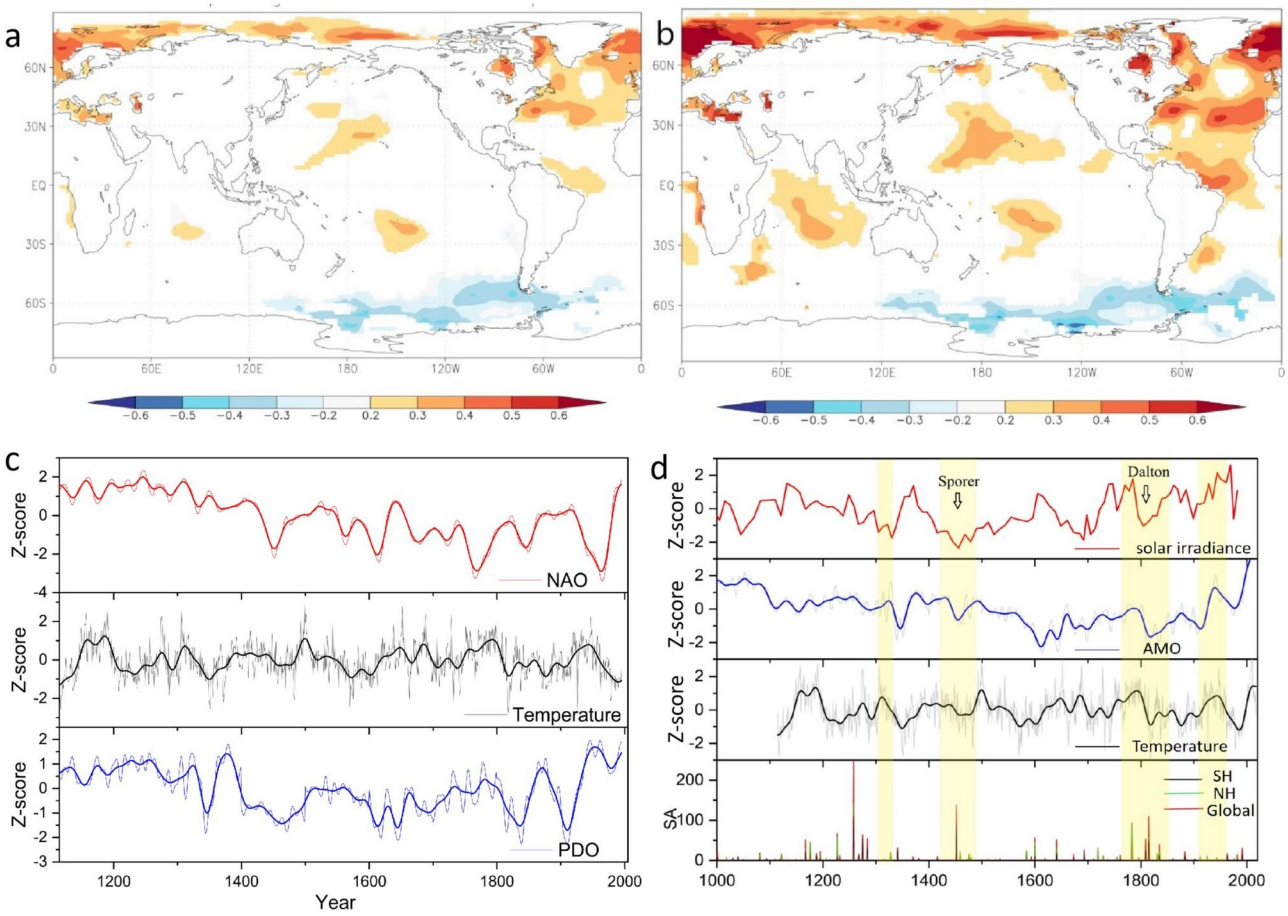

Fig. 6. Exploration of possible linkages between reconstructed temperature and external forcing factors. (**a**) Correlation patterns of our reconstructed temperature with the concurrent NCDC V5 SST data for the annual and (**b**) 21-year running mean data during the period 1959–2017. The figures are created at http://climexp.knmi.nl. Comparison of our annual temperature (black line) with (**c**) the North Atlantic Oscillation (NAO, red line) and Pacific Decadal Oscillation (PDO, blue line), and with (**d**) Total Solar Irradiance (red line), Atlantic Multidecadal Oscillation (AMO, blue line), sulfate aerosol concentration. The labels SH, NH, and global indicate volcanic events in the Southern Hemisphere, Northern Hemisphere, and globally, respectively. All sequences also pass through an 11-year moving average.

36, 18, 7 and 2–2.6 years. External forcing factors such as volcanic eruption, AMO and solar activity significantly influence temperature variations.

Materials and methods

Study area

The study area (100.50°-100.80°E, 29.03°-30.13°N) is located on Haizi mountain, southeastern TP, China, with the average elevation of 4500 m (Fig. 1). The Eastern Asian monsoon, Indian monsoon, and the continental westerlies play an active role in driving the regional climate patterns of this region[74]. According to the record from 1958–2017 at the Daocheng meteorological station (29.03°N, 100.18°E, 3728 m a.s.l.), the mean annual temperature is about 4.58℃, with the warmest and coldest months being June (12.3℃) and December (-15.3℃), respectively. The average annual precipitation is around 660 mm, with 94% of it falling between May and September. The vegetation in this region is typical of a subalpine coniferous forest[17]. *Picea likiangensis* and *Juniperus saltuaria* are the dominant species in the incised valley, *Rhododendron decorum* Franch. and *Rhododendron phaeochrysum* are found in the understory. *Juniperus saltuaria* is distributed on the plateau surface at altitudes of 4500–4600 m a.s.l. in the form of isolated tree or small patches, *Rhododendron aganniphum* var. *aganniphum*are found in the understory.

Tree-ring dataset

In total, 73 cores from 30 living trees were extracted using increment borers, and 20 discs were obtained from dead trees. The tree species investigated was *Juniperus saltuaria*, which has long tree-age, clear ring boundaries and suitable for dendrochronology study. According to international standard techniques, the samples were dried and sanded with progressively finer grades of abrasive paper. Skeleton plots and TSAP-win standard annual ring analysis software were used for cross-dating. Tree-ring widths were measured with a Lintab 6 system (Rinntech,

Eruption year	Eruption month	Eruption days	Latitude	Volcano name	VEI	−1	0	+1	+2	+3
1886	6	10	−38.12	Okataina (Tarawera)	5	−0.98	1.62	−1.17	1.24	0.52
1883	8	27	−6.10	Krakatau	6	0.12	0.71	0.06	−0.98	1.62
1875	4	1	65.03	Askja1	5	−0.81	0.20	−0.44	−0.51	0.25
1835	1	20	12.98	Cosigüina	5	−0.28	0.78	−0.91	−1.33	0.92
1822	10	8	−7.25	Galunggung	5	−0.21	−0.27	0.73	0.05	0.33
1815	4	10	−8.25	Tambora2	7	1.61	−2.31	0.58	−2.12	−0.09
1755	10	17	63.63	Katla	5	−0.61	−1.01	1.04	−0.73	1.20
1739	8	19	42.69	Shikotsu (Tarumai)	5	0	−0.45	−1.61	0.12	0.16
1721	5	11	63.63	Katla1	5	−0.28	0.87	0.17	0.08	−1.04
1707	12	16	35.36	Fujisan	5	2.25	−1.49	0.74	−0.97	−0.80
1673	5	20	1.38	Gamkonora	5	0.98	−0.14	−0.72	−0.99	0.62
1667	9	23	42.69	Shikotsu (Tarumai)	5	1.09	−0.70	−0.20	0.04	1.22
1640	12	26	6.11	Parker	5	−1.43	0.39	−1.26	0.39	0.24
1600	2	17	−16.61	Huaynaputina	6	0.32	−0.91	−0.13	1.05	−1.12
1477	2	1	64.63	Bárðarbunga	6	1.02	−0.22	−0.75	1,19	−0.87
1257	7(±3)	-	−8.42	Rinjani (Samalas)	7	2.57	−0.93	−0.17	−0.61	−0.31

Table 5. Data of Volcanic eruption events (Eruption dates, Volcano latitude, Volcano names and volcanic explosivity index (VEI)) and the first differences of reconstructed temperature in the year before (-1), during (0) and the following three years (+1, +2, +3) after the eruption.

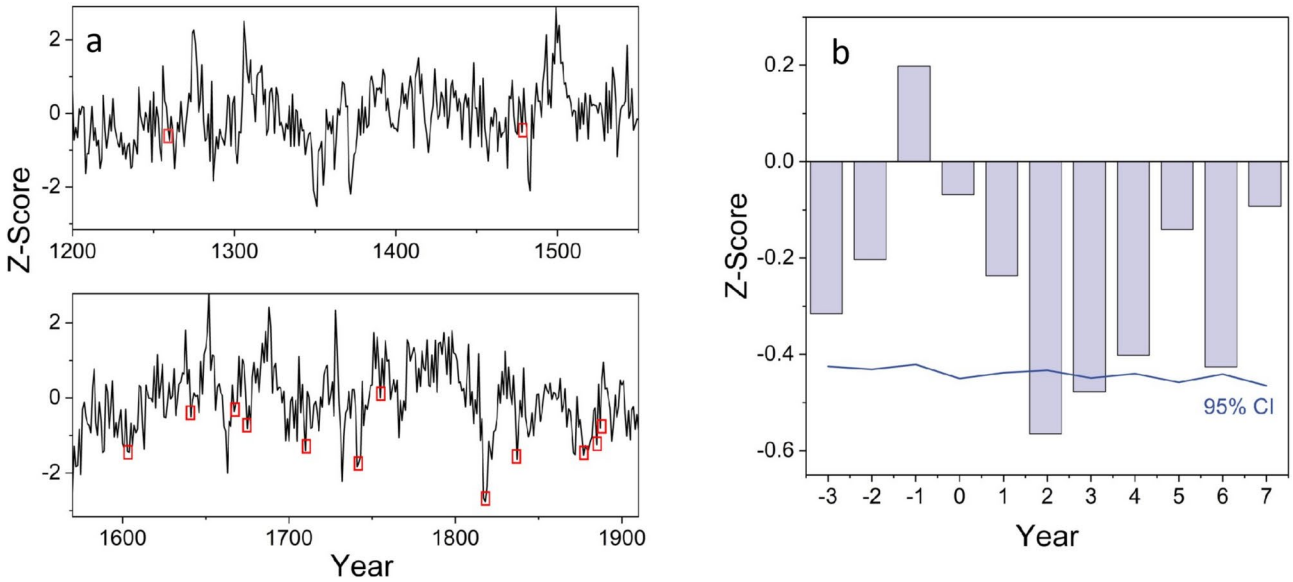

Fig. 7. (a) Relationship between the interannual variations in the reconstructed temperature and volcanic eruptions The red boxes indicate low temperature values, each following a volcanic eruption event. (b) SEA results of our reconstructed T_{mean} with large volcanic eruptions during 1115–1017 CE. 0: year of volcanic eruption; -1: year before eruption; 1: year after eruption. The solid line represents the 95% confidence limits using Monte Carlo-type block bootstrapping.

Heidelberg, Germany) at a resolution of 0.001 mm. Depending on the specific conditions of these samples, 1-3 directions of each disc were selected to measure. Then, the COFECHA[75]software (2012) was utilized to check results of cross-dating and corrected errors following microscopic examination of the tree-ring characteristics. A 67% of the series length cubic spline function was applied to remove the age-related trend for each series using the ARSTAN program[76]. The bi-weight robust estimation of mean was employed for all the detrended series to produce STD, residual chronology (RES) and arstan chronology (ARS). The strongest correlation calculation existed between STD and ARS (0.929, $P<0.01$), but a relatively low correlation was observed between STD and RES (0.676, $P<0.01$). Because the standard chronology can maximize low- to high-frequency common variance, presumably in response to climate, STD was chosen for subsequent analysis[30]. The mean sensitivity (MS), standard deviation (SD) and first-order autocorrelation coefficient (AC1) of the chronology were calculated to assess the quality of the chronology. The SNR and the PC1 also were calculated. In addition, the common

interval analysis was carried out for the period from 1640 to 1990 CE. The subsample signal strength (SSS)[77] with a cutoff value of 0.85 was used to assess the reliability of chronology like many other studies reported for the southeastern TP[78]. The threshold corresponded a sample depth of 11 trees (from 1115 CE). All the analyses were completed in the Tree Ring Laboratory, School of Geographical Sciences, Nanjing Normal University.

Climate data

The nearest meteorological station is Yading Airport station, but there is only data from 2015 CE, so we download the meteorological data from other stations in the region (Daocheng, Litang, Batang and Derong). As Daocheng station (29.03°N, 100.18°E, 3728 m a.s.l.) is much closer to our sampling sites, which is located 52 km from our sampling sites, the meteorological data (precipitation (P), mean temperature (T_{mean}), mean minimum temperature (T_{min}), and mean maximum temperature (T_{max})) of this station were selected for subsequent correlation analysis (Data from https://data.cma.cn/, accessed on 24 April 2023). We investigated the climate-t ree growth relationships between monthly/seasonal/annual climate variables and tree ring width index using Pearson correlation analyses. Then, a simple linear regression equation was used for T_{mean} reconstruction. Because the climate record is only 67 years which is not long enough to be divided into the calibration and verification sections, independent data were generated using the 'leave-one-out' method to evaluate the goodness-of-fit of the model[79]. Verification statistics used included the explained variance (R^2), the sign test (ST), the reduction of error statistic (RE), the product means test (T)[14].

Statistical analysis

We employed MTM of spectral analysis to identify the periodicities of the reconstructed temperature[80]. To illustrate the geographical representation of our temperature record, we performed spatial correlations between our reconstruction and the Climate Research Unit (CRU TS4.08, 0.5°×0.5°) gridded temperature dataset for the period 1957–2017 and 1901–2017. Addition, the correlation after removing linear trends from the data using the detrending feature of the KNMI Climate Explorer[39] (http://www.knmi.nl) was also computed. Additionally, we employed superposed epoch analysis[81] (SEA) to evaluate the impact of volcanic forcing.

Data availability

The datasets generated during and/or analyzed during the current study are available from the supplement.

Received: 12 July 2024; Accepted: 6 November 2024
Published online: 11 November 2024

References

1. PAGES 2k Consortium. Consistent multidecadal variability in global temperature reconstructions and simulations over the Common Era. *Nat. Geosci.* **12**, 643–649 (2019).
2. Chen, F. et al. Role of Pacific Ocean climate in regulating runoff in the source areas of water transfer projects on the Pacific Rim. *Npj Clim. Atmospheric Sci.* **7**, 1–9 (2024).
3. Jones, P. D. & Mann, M. E. Climate over past millennia. *Rev. Geophys.* **42**, (2004).
4. Wang, Q., Fan, X. & Wang, M. Recent warming amplification over high elevation regions across the globe. *Clim. Dyn.* **43**, 87–101 (2014).
5. Liu, T. et al. Teleconnections among tipping elements in the Earth system. *Nat. Clim. Change* **13**, 67–74 (2023).
6. Du, Z. & Tandong, Y. Uplifting of Tibetan Plateau with Its Environmental Effects. *Adv. Earth Sci.* **21**, 451 (2006).
7. Yu, J. et al. Summer temperature variability inferred from tree-ring records in the central Hengduan Mountains, southeastern Tibetan Plateau. *Dendrochronologia* **51**, 92–100 (2018).
8. Chen, F. et al. Ecological and societal effects of Central Asian streamflow variation over the past eight centuries. *Npj Clim. Atmospheric Sci.* **5**, 27 (2022).
9. Chen, F., He, Q., Bakytbek, E., Yu, S. & Zhang, R. Reconstruction of a long streamflow record using tree rings in the upper Kurshab River (Pamir-Alai Mountains) and its application to water resources management. *Int. J. Water Resour. Dev.* **33**, 976–986 (2017).
10. Chen, F. et al. 500-year tree-ring reconstruction of Salween River streamflow related to the history of water supply in Southeast Asia. *Clim. Dyn.* **53**, 6595–6607 (2019).
11. Chen, Y., Chen, F. & Zhang, H. A Tree-Ring-Based Precipitation Reconstruction since 1760 CE from Northeastern Tibetan Plateau. *China. Atmosphere* **12**, 416 (2021).
12. Chen, F. et al. Coupled Pacific Rim megadroughts contributed to the fall of the Ming Dynasty's capital in 1644 CE. *Sci. Bull.* **69**, 3106–3114 (2024).
13. Chen, F. et al. Southeast Asian ecological dependency on Tibetan Plateau streamflow over the last millennium. *Nat. Geosci.* https://doi.org/10.1038/s41561-023-01320-1 (2023).
14. Fritts HC. Tree-Rings and Climate. *Elsevier* (1976).
15. Keyimu, M. et al. Tree-ring based minimum temperature reconstruction on the southeastern Tibetan Plateau. *Quat. Sci. Rev.* **251**, 106712 (2021).
16. Lin, Z. Y. & Wu, X. D. A preliminary analysis about the tracks of moisture transportation in the Qinghai-Xizang Plateau. *Geogr. Res.* **9**, 33–40 (1990).
17. Yin, X., Zhao, F., Wu, J., Liu, H. & Wen, L. Main Vegetation Types in Yading Nature Reserve, Daocheng County, Sichuan Province. *J. Sichuan For. Sci. Technol.* **34**, 50–54 (2013).
18. Huang, R. et al. A tree ring-based winter temperature reconstruction for the southeastern Tibetan Plateau since 1340 CE. *Clim. Dyn.* **53**, 3221–3233 (2019).
19. Liang, E., Shao, X. & Liu, X. Annual Precipitation Variation Inferred from Tree Rings Since A.D. 1770 for the Western Qilian Mts., Northern Tibetan Plateau. *Tree-Ring Res.* **65**, 95–103 (2009).
20. Yang, B., Kang, X., Liu, J., Bräuning, A. & Qin, C. Annual temperature history in Southwest Tibet during the last 400 years recorded by tree rings: ANNUAL TEMPERATURE HISTORY IN SOUTHWEST TIBET. *Int. J. Climatol.* **30**, 962–971 (2010).
21. Zhu, H.-F. et al. August temperature variability in the southeastern Tibetan Plateau since AD 1385 inferred from tree rings. *Palaeogeogr. Palaeoclimatol. Palaeoecol.* **305**, 84–92 (2011).
22. Lv, L. & Zhang, Q. Tree-ring based summer minimum temperature reconstruction for the southern edge of the Qinghai-Tibetan Plateau. *China. Clim. Res.* **56**, 91–101 (2013).

23. Wang, J. et al. Tree-ring inferred annual mean temperature variations on the southeastern Tibetan Plateau during the last millennium and their relationships with the Atlantic Multidecadal Oscillation. *Clim. Dyn.* **43**, 627–640 (2014).
24. Deng, X. & Zhang, Q.-B. Tree growth and climate sensitivity in open and closed forests of the southeastern Tibetan Plateau. *Dendrochronologia* **33**, 25–30 (2015).
25. Fang, K. et al. Interdecadal modulation of the Atlantic Multi-decadal Oscillation (AMO) on southwest China's temperature over the past 250 years. *Clim. Dyn.* **52**, 2055–2065 (2019).
26. Zou, L., Xu, S. & Zheng, C. Relationship between the tree ring width of Sabina saltuaria and climate factors in Haizi Mountain, Daocheng. *Sichuan. J. Glaciol. Geocryol.* **43**, 917–927 (2021).
27. Bräuning, A. Dendrochronology for the last 1400 years in eastern Tibet. *GeoJournal* **34**, 75–95 (1994).
28. Li, T. *et al.* Dendroclimatological study of Sabina saltuaria and Abies faxoniana in the mixed forests of the Qionglai Mountains, eastern Tibetan Plateau. *J. For. Res.* **35**, (2024).
29. Cui, L. et al. The recent high occurrence of spring atmospheric droughts over central Hengduan Mountains is unprecedented in 669-year tree-ring records. *Palaeogeogr. Palaeoclimatol. Palaeoecol.* **649**, 112318 (2024).
30. Li, Z., Liu, G., Wu, X. & Wang, X. Tree-ring-based temperature reconstruction for the Wolong Natural Reserve, western Sichuan Plateau of China: A TEMPERATURE RECONSTRUCTION IN SOUTHWESTERN CHINA FROM TREE RINGS. *Int. J. Climatol.* **35**, 3296–3307 (2015).
31. Deslauriers, A., Rossi, S., Anfodillo, T. & Saracino, A. Cambial phenology, wood formation and temperature thresholds in two contrasting years at high altitude in southern Italy. *Tree Physiol.* **28**, 863–871 (2008).
32. Liang, E., Wang, Y., Xu, Y., Liu, B. & Shao, X. Growth variation in Abies georgei var. smithii along altitudinal gradients in the Sygera Mountains, southeastern Tibetan Plateau. *Trees* **24**, 363–373 (2010).
33. Misson, L., Rathgeber, C. & Guiot, J. Dendroecological analysis of climatic effects on Quercus petraea and Pinus halepensis radial growth using the process-based MAIDEN model. *Can. J. For. Res.* **34**, 888–898 (2004).
34. Dang, H., Zhang, Y., Zhang, K., Jiang, M. & Zhang, Q. Climate-growth relationships of subalpine fir (Abies fargesii) across the altitudinal range in the Shennongjia Mountains, central China. *Clim. Change* **117**, 903–917 (2013).
35. Shah, S. K., Pandey, U., Mehrotra, N., Wiles, G. C. & Chandra, R. A winter temperature reconstruction for the Lidder Valley, Kashmir, Northwest Himalaya based on tree-rings of Pinus wallichiana. *Clim. Dyn.* **53**, 4059–4075 (2019).
36. Gaire, N. P. et al. Abies spectabilis shows stable growth relations to temperature, but changing response to moisture conditions along an elevation gradient in the central Himalaya. *Dendrochronologia* **60**, 125675 (2020).
37. Fan, Z.-X., Bräuning, A., Tian, Q.-H., Yang, B. & Cao, K.-F. Tree ring recorded May–August temperature variations since A.D. 1585 in the Gaoligong Mountains, southeastern Tibetan Plateau. *Palaeogeogr. Palaeoclimatol. Palaeoecol.* **296**, 94–102 (2010).
38. Li, Z.-S., Zhang, Q.-B. & Ma, K. Tree-ring reconstruction of summer temperature for A.D. 1475–2003 in the central Hengduan Mountains, Northwestern Yunnan, China. *Clim. Change* **110**, 455–467 (2012).
39. Trouet, V. & Van Oldenborgh, G. J. KNMI Climate Explorer: A Web-Based Research Tool for High-Resolution Paleoclimatology. *Tree-Ring Res.* **69**, 3–13 (2013).
40. Shao, X. M. & Fan, J. Past Climate On West Sichuan Plateau As Reconstructed From Ring-Widths Of Dragon Spruce. *Quaternary Sciences* **1**, 311 (1999).
41. Deng, Y., Gou, X., Gao, L., Yang, T. & Yang, M. Early-summer temperature variations over the past 563 yr inferred from tree rings in the Shaluli Mountains, southeastern Tibet Plateau. *Quat. Res.* **81**, 513–519 (2014).
42. Bräuning, A. Summer temperature and summer monsoon history on the Tibetan plateau during the last 400 years recorded by tree rings. *Geophys. Res. Lett.* **31**, L24205 (2004).
43. Yang, B. et al. A 622-year regional temperature history of southeast Tibet derived from tree rings. *The Holocene* **20**, 181–190 (2010).
44. Wang, Y., Liang, E., Ellison, A. M., Lu, X. & Camarero, J. J. Facilitation stabilizes moisture-controlled alpine juniper shrublines in the central Tibetan Plateau. *Glob. Planet. Change* **132**, 20–30 (2015).
45. PAGES Asia2k Members *et al.* Tree-ring reconstructed summer temperature anomalies for temperate East Asia since 800 C.E. *Clim. Dyn.* **41**, 2957–2972 (2013).
46. Wilson, R. et al. Last millennium northern hemisphere summer temperatures from tree rings: Part I: The long term context. *Quat. Sci. Rev.* **134**, 1–18 (2016).
47. You, Q. *et al.* Tibetan Plateau amplification of climate extremes under global warming of 1.5 °C, 2 °C and 3 °C. *Glob. Planet. Change* **192**, 103261 (2020).
48. Zhu, K. A preliminary study of climate change in China over the past 5,000 years. *Sci. China Earth Sci.* **3**, 168–189 (1973).
49. Cai, W. & Yin, S. The Freeze Disasters in the Little Ice Age of Ming and Qing Dynasties in the Guanzhong Region. *J. Arid Land Resour. Environ.* **23**, 118–121 (2009).
50. Cook, E. R., Krusic, P. J. & Jones, P. D. Dendroclimatic signals in long tree-ring chronologies from the Himalayas of Nepal. *Int. J. Climatol.* **23**, 707–732 (2003).
51. Qin, N., Shao, X., Li, Y. & Li, J. Annual temperature recorded in tree-ring from Songpan region. *Chin. Sci. Bull.* **59**, 1446–1458 (2014).
52. Wu, P., Wang, L. & Shao, X. Reconstruction of summer temperature variation from maximum density of alpine pine during 1917–2002 for west Sichuan Plateau. *China. J. Geogr. Sci.* **18**, 201–210 (2008).
53. Shi, C. et al. Summer Temperature over the Tibetan Plateau Modulated by Atlantic Multidecadal Variability. *J. Clim.* **32**, 4055–4067 (2019).
54. Sun, W. et al. Impacts ofmajor volcanic eruptions over the past two millennia on both global and Chinese climates: Areview. *Sci. China Earth Sci.* **54**, 64–82 (2024).
55. Yuan, Q., Yu, S., Jiang, S., Qin, N. & Zhang, T. Tree-ring reconstruction of March-August drought variability over the past 567 years in the Yajiang region of West Sichuan Plateau. *China. Chin. J. Appl. Ecol.* **32**, 3627–3635 (2021).
56. Li, T. & Li, J. A 564-year annual minimum temperature reconstruction for the east central Tibetan Plateau from tree rings. *Glob. Planet. Change* **157**, 165–173 (2017).
57. Ge, Q., Hao, Z., Zheng, J. & Shao, X. Temperature changes over the past 2000 yr in China and comparison with the Northern Hemisphere. *Clim. Past* **9**, 1153–1160 (2013).
58. Yao, T. et al. Recent Third Pole's Rapid Warming Accompanies Cryospheric Melt and Water Cycle Intensification and Interactions between Monsoon and Environment: Multidisciplinary Approach with Observations, Modeling, and Analysis. *Bull. Am. Meteorol. Soc.* **100**, 423–444 (2019).
59. Mann, M. E. et al. Proxy-based reconstructions of hemispheric and global surface temperature variations over the past two millennia. *Proc. Natl. Acad. Sci. U. S. A.* **105**, 13252–13257 (2008).
60. Mann, M. E. et al. Global Signatures and Dynamical Origins of the Little Ice Age and Medieval Climate Anomaly. *Science* **326**, 1256–1260 (2009).
61. Gray, L. J. *et al.* SOLAR INFLUENCES ON CLIMATE. *Rev. Geophys.* **48**, RG4001 (2010).
62. Anchukaitis, K. J. *et al.* Influence of volcanic eruptions on the climate of the Asian monsoon region: VOLCANOES AND THE ASIAN MONSOON. *Geophys. Res. Lett.* **37**, n/a-n/a (2010).
63. Grossmann, I. & Klotzbach, P. J. A review of North Atlantic modes of natural variability and their driving mechanisms. *J. Geophys. Res. Atmospheres* **114**, (2009).
64. Li, S. & Bates, G. T. Influence of the Atlantic Multidecadal Oscillation on the winter climate of East China. *Adv. Atmospheric Sci.* **24**, 126–135 (2007).

65. Li, S., Perlwitz, J., Quan, X. & Hoerling, M. P. Modelling the influence of North Atlantic multidecadal warmth on the Indian summer rainfall. *Geophys. Res. Lett.* **35**, (2008).
66. Shi, F., Ting, M. & Guo, Z. Quantitative attribution of Northern Hemisphere temperatures over the past 2000 years. *Front. Earth Sci.* https://doi.org/10.1007/s11707-023-1086-6 (2023).
67. Wang, Y., Shao, X., Zhang, Y. & Li, M. The response of annual minimum temperature on the eastern central Tibetan Plateau to large volcanic eruptions over the period 1380–2014 CE. *Clim. Past* **17**, 241–252 (2021).
68. Sigl, M. et al. Timing and climate forcing of volcanic eruptions for the past 2,500 years. *Nature* **523**, 543–549 (2015).
69. Chen, F., Wang, H. & Yuan, Y. Two centuries of temperature variation and volcanic forcing reconstructed for the northern Tibetan Plateau. *Phys. Geogr.* **38**, 248–262 (2017).
70. Pinker, R. T., Zhang, B. & Dutton, E. G. Do Satellites Detect Trends in Surface Solar Radiation?. *Science* **308**, 850–854 (2005).
71. Sun, C. et al. Sunshine duration reconstruction in the southeastern Tibetan Plateau based on tree-ring width and its relationship to volcanic eruptions. *Sci. Total Environ.* **628–629**, 707–714 (2018).
72. Delaygue, G. & Bard, E. An Antarctic view of Beryllium-10 and solar activity for the past millennium. *Clim. Dyn.* **36**, 2201–2218 (2011).
73. Song, A., Liu, S., Shi, Z. & Dong, L. Quantitative classification and ordination of subalpine meadow in Wolong Nature Reserve. *Ying Yong Sheng Tai Xue Bao J. Appl. Ecol.* **17**, 1174–1178 (2006).
74. Holmes, R. L. COMPUTER -ASSISTED QUALITY CONTROL IN TREE -RING DATING AND MEASUREMENT. 11.
75. Cook, E. R. A TIME SERTES ANALYSIS APPROACH TO TREE RING STANDARDIZATION. (1985).
76. Wigley, T. M. L., Briffa, K. R. & Jones, P. D. On the Average Value of Correlated Time Series, with Applications in Dendroclimatology and Hydrometeorology. *J. Appl. Meteorol. Climatol.* **23**, 201–213 (1984).
77. Fang, K. et al. Reconstructed droughts for the southeastern Tibetan Plateau over the past 568 years and its linkages to the Pacific and Atlantic Ocean climate variability. *Clim. Dyn.* **35**, 577–585 (2010).
78. Blasing, T. J., Duvick, D. N. & West, D. C. *Dendroclimatic calibration and verification using regionally averaged and single station precipitation data* (Tree Ring Bull, 1981).
79. Mann, M. E. & Lees, J. M. Robust estimation of background noise and signal detection in climatic time series. *Clim. Change* **33**, 409–445 (1996).
80. Haurwitz, M. W. & Brier, G. W. A Critique of the Superposed Epoch Analysis Method: Its Application to Solar-Weather Relations. *Mon. Weather Rev.* **109**, 2074–2079 (1981).

Acknowledgements

We gratefully acknowledge all the staff of Nature Reserve Management Unit of the Forestry and Grassland Bureau of Daocheng County. Thanks to other members of our team for their help during sampling.

Author contributions

All authors contributed to the study conception and design. Material preparation and data collection were performed by Shanshan Xu, Chaogang Zheng, Zhigang Zhang, Zhijun Zhao and Xinggong Kong, data analysis was performed by Shanshan Xu, Lili Zou and Zhiyuan Shang. The first draft of the manuscript was written by Shanshan Xu. Zhiyuan Shang and Iain Robertson is responsible for polishing the entire text and correcting grammar errors. And all authors commented on previous versions of the manuscript. All authors read and approved the final manuscript.

Funding

This research was funded by the National Natural Science Foundation of China (41971009), the Strategic Priority Research Program (A) of the Chinese Academy of Sciences (XDA20100300); and the Second Tibetan Plateau Scientific Expedition Program (STEP) (2019QZKK0205).

Competing interests

The authors have no relevant financial or non-financial interests to disclose.

Additional information

Supplementary Information The online version contains supplementary material available at https://doi.org/10.1038/s41598-024-79096-6.

Correspondence and requests for materials should be addressed to Z.S. or Z.Z.